

1  
2 **Wavelet Analysis for Non-stationary, Non-linear Time Series**

3 **Justin A. Schulte**

4 **The Pennsylvania State University, University Park,**  
5 **Pennsylvania 16802**

6 **Abstract**

7 Methods for detecting and quantifying nonlinearities in nonstationary time series are introduced  
8 and developed. In particular, higher-order wavelet analysis was applied to an ideal time series and  
9 the Quasi-biennial Oscillation (QBO) time series. Multiple-testing problems inherent in wavelet  
10 analysis were addressed by controlling the false discovery rate. A new local autobicoherence  
11 spectrum facilitated the detection of local nonlinearities and the quantification of cycle geometry.  
12 The local autobicoherence spectrum of the QBO time series showed that the QBO time series  
13 contained a mode with a period of 28 months that was phase-coupled to a harmonic with a period  
14 of 14 months. An additional nonlinearly interacting triad was found among modes with periods of  
15 10, 16, 26 months. Local biphase spectra determined that the nonlinear interactions were not  
16 quadratic and that the effect of the nonlinearities was to produce non-smoothly varying  
17 oscillations. The oscillations were found to be skewed so that negative QBO regimes were  
18 preferred, and also asymmetric in the sense that phase transitions between the easterly and westerly  
19 phases occurred more rapidly than those from westerly to easterly regimes.

20 **1. Introduction**

21 Spectral analysis is a tool for extracting embedded structures in a time series. In particular,  
22 Fourier analysis has been used extensively by researchers for extracting deterministic structures  
23 from time series but is incapable of detecting nonstationary features often present in geophysical  
24 time series. Wavelet analysis can extract transient features embedded in time series, with a wavelet  
25 power spectrum representing variance (power) of a time series as a function of time and period.  
26 Since the seminal work of Torrence and Compo (1998), wavelet analysis has been applied  
27 extensively to geophysical time series such as the indices for the North Atlantic Oscillation (Olsen  
28 et al., 2012), Arctic Oscillation (Jevrejeva et al., 2003), Pacific Decadal Oscillation (Macdonald

1 and Case, 2005; Newmann et al., 2003), El-Niño/Southern Oscillation (ENSO; Torrence and  
2 Webster, 1999), Pacific-North American Pattern, and West Pacific pattern (Gan et al., 2007). The  
3 application of wavelet coherence and cross-wavelet analyses (Grinsted et al., 2004), moreover, has  
4 proven useful in relating geophysical time series to other time series (Jevrejeva et al., 2003; Gan  
5 et al., 2007; Labat, 2010; Lee and Lwiza, 2008).

6 Many statistical methods, including power and cross-spectral analyses, rely on the assumption  
7 that the variable in question is Gaussian distributed (King, 1996). For a linear system in which the  
8 output is proportional to the input, the first- and second-order moments, the mean and variance,  
9 can fully describe the distribution of a process. In the frequency domain, by analogy, the variable  
10 can be fully described by the power spectrum, the decomposition of variance as a function of  
11 frequency. Suppose, however, that the distribution is non-Gaussian so that higher-order moments  
12 such as skewness and kurtosis exist. In this case, the mean and variance, while useful, are unable  
13 to fully describe the distribution in question. In a time series context, non-Gaussian distributions  
14 can arise from nonlinear systems, systems for which the output is no longer simply proportional  
15 to the input. For a nonlinear system, if the input is the sum of two sinusoids with different  
16 frequency components the output will contain additional frequency components representing the  
17 sum and difference of the input frequencies (King, 1996). In such cases, it is necessary to examine  
18 the decomposition of higher-order moments in frequency space.

19 The frequency decomposition of the third-order moment, for example, results in a bispectrum  
20 or skewness function that measure deviations from Gaussianity (Nikias and Raghuvver, 1987;  
21 King, 1996). In fact, Hinich (1985) developed a bispectral test to determine if a time series is non-  
22 Gaussian and nonlinear. In some situations, higher-order nonlinearities such as cubic nonlinearities  
23 may exist, in which case the trispectrum or other polyspectra would have to be used (Collis et al.,  
24 1998).

25 Another advantage of higher-order spectral analysis is that the cycle geometry of oscillations,  
26 such as asymmetry with respect to a horizontal axis (skewed oscillation) or with respect to a  
27 vertical axis (asymmetric oscillation) can be quantified using the biphase. A pure sine wave, for  
28 example, is neither skewed nor asymmetric, whereas a time series resembling a saw-tooth is  
29 asymmetric. Skewed and asymmetric cycle geometry can identify, for example, abrupt climatic  
30 shifts, sudden shifts in the climate system that exceed the magnitude of the background variability

1 (King, 1996). Abrupt climate shifts have occurred numerous times in the past and have dire  
2 impacts on ecological and economic systems (Alley et al., 2005). An understanding of past abrupt  
3 climate shifts is essential to understanding future climate change and so there is a need to quantify  
4 nonlinearities present in climatic oscillations.

5 The Quasi-biennial Oscillation (QBO), as another example, has been shown to behave  
6 nonlinearly, transitioning from easterly phases to westerly phases more rapidly than from westerly  
7 to easterly phases (Lu et al., 2009). Another source of asymmetry in the QBO time series arises  
8 from the westerly shear zone descending more regularly than the easterly shear zone. Asymmetries  
9 in the QBO time series are not well-captured by linear methods such as linear principal component  
10 and singular spectrum analyses (Lu et al., 2009) but are better captured using, for example,  
11 nonlinear principal component analysis (Hamilton and Hsieh, 2002). Another example of a  
12 nonlinear time series is the sunspot cycle. Solar activity undergoes an 11-year oscillation  
13 characterized by asymmetric cycle geometry, with solar maxima generally rising faster than they  
14 fall, indicating the presence of nonlinearities (Moussas et al., 2005; Rusu, 2007). ENSO, a climate  
15 phenomenon with regional- to global-scale impacts, has also been shown to exhibit nonlinearities  
16 (Timmermann, 2003). The presence of nonlinearities and possible nonstationarities in the QBO,  
17 ENSO, and sunspot time series makes traditional Fourier and wavelet analysis inadequate for  
18 feature extraction, underscoring the need to develop methods for quantifying nonlinearities in a  
19 nonstationary geophysical setting.

20 The application of higher-order wavelet analysis has been rather limited compared to  
21 traditional wavelet analysis (van Millagan et al., 1995; Elsayed, 2006). One geophysical  
22 application of higher-order wavelet analysis is to oceanic waves (Elsayed, 2006), which was found  
23 to be capable of identifying nonlinearities in wind-wave interactions. However, the study lacked  
24 rigorous statistical significance testing, which is problematic because even a Gaussian process of  
25 finite length can produce nonzero bicoherence. Therefore, the first aspect of this paper is to apply  
26 significance testing methods for higher-order wavelet analysis to aid physical interpretation of  
27 results.

28 The number of bicoherence estimates to which the statistical test is applied will be large and  
29 multiple artifacts will result. The multiple-testing problem was already identified for traditional  
30 wavelet analysis (Maraun et al., 2007; Schulte et al., 2015, Schulte, 2016). The first objective of

1 this paper will be therefore to apply statistical methods controlling false positive detection. It is  
2 also noted that the bicoherence spectra calculated are only sample estimates of the true bicoherence  
3 spectra. The second objective of this paper will be to develop a procedure for calculating  
4 confidence intervals corresponding to the sample estimates, which represent a range of plausible  
5 values for the sample estimates.

6 Another problem with the application of higher-order wavelet analysis is selection of a time  
7 interval on which to calculate the high-order wavelet quantities. Such an approach is subjective  
8 and the result of the analysis may depend on the time interval chosen. Objective three of this paper  
9 will address the time interval selection problem. Such an approach has already been adopted in  
10 wavelet coherence analysis (Grinsted et al., 2004).

11 Additionally, properties of the biphase have only been examined for Fourier-based bispectral  
12 analysis (Elgar and Sebert, 1989; Maccarone, 2013) and its usefulness in higher-order wavelet  
13 analysis has yet to be examined. For nonstationary time series, the biphase and cycle geometry  
14 corresponding to the time series may change with time and thus objective four of this paper will  
15 be to introduce a local wavelet-based biphase spectrum.

16 In this paper, higher-order wavelet analysis is put in a statistical framework and applied to the  
17 QBO time series to demonstrate the insights afforded by the methods. Before describing higher-  
18 wavelet analysis, a brief overview of wavelet analysis is first presented in Sect. 2. Higher-order  
19 wavelet analysis is described in Sect. 3 and a new local autobicoherence spectrum is introduced,  
20 eliminating the selection of a time interval on which to calculate nonlinear properties of time series.  
21 The new and existing methods are applied to an ideal time series and the QBO index. In Section  
22 4, a new procedure for estimating confidence intervals of global autobicoherence quantities is  
23 developed to estimate uncertainties in the sample autobicoherence spectra. The application of the  
24 new procedure to the sample autobicoherence spectrum of the QBO time series is then used to  
25 further assess confidence in results.

## 26 **2. Wavelet Analysis**

27 The idea behind wavelet analysis is to convolve a time series with a function satisfying certain  
28 conditions. Such functions are called wavelets, of which the most widely used is the Morlet  
29 wavelet, a sinusoid damped by a Gaussian envelope:

1 
$$\psi_0(\eta) = \pi^{-1/4} e^{i\omega_0\eta} e^{-\frac{1}{2}\eta^2}, \quad (1)$$

2 where  $\psi_0$  is the Morlet wavelet,  $\omega_0$  is the dimensionless frequency, and  $\eta$  is the dimensionless  
 3 time (Torrence and Compo, 1998; Grinsted et al., 2004). In practical applications, the convolution  
 4 of the wavelet function with a time series  $X = (x_n; n = 1, \dots, N)$  is calculated discretely using

5 
$$W_n^X(s) = \sqrt{\frac{\delta t}{s}} \sum_{n'=1}^N x_{n'} \psi_0[(n' - n) \frac{\delta t}{s}], \quad (2)$$

6 where  $\delta t$  is a uniform time step,  $s$  is scale,  $\eta = s \cdot t$ , and  $W_n^X(s)$  is the wavelet transform. The  
 7 wavelet power is given by  $|W_n^X(s)|^2$  (Torrence and Compo, 1998; Grinsted et al., 2004). For the  
 8 Morlet wavelet with  $\omega_0 = 6$ , the wavelet scale and the Fourier period  $\lambda$  are approximately equal  
 9 ( $\lambda = 1.03s$ ). A more detailed discussion of wavelet analysis can be found in Torrence and Compo  
 10 (1998).

11 Shown in Fig. 1a is the time series of the QBO index and shown in Fig. 1b is the  
 12 corresponding wavelet power spectrum. The QBO data from 1950-2013 were obtained from the  
 13 Climate Prediction Center. The QBO index is defined as the zonal average of the 30 hPa zonal  
 14 wind at the equator. As such, a positive index indicates westerly winds and a negative index  
 15 indicates easterly winds. The most salient feature of the time series is the rather regular periodicity  
 16 of approximately 28 months. Also note the asymmetry between the negative and positive phase,  
 17 with the negative phases generally being stronger. The periodic behavior of the QBO was  
 18 corroborated by examining the wavelet power spectrum. A well-defined 28-month periodicity is  
 19 evident, with the associated wavelet power changing little throughout the study period.

20 There are also secondary features located at a period of approximately 14 months, primarily  
 21 from 1985 to 2013. The appearance of significant power at a period of 14 months also coincides  
 22 with most of the largest negative phases of the QBO. Such a correspondence may not have been a  
 23 coincidence; the 14-month mode and the 28-month mode may have interacted constructively to  
 24 generate large negative events but interacted destructively to create smaller positive events.  
 25 However, additional tools are needed to confirm if the periodicities are interacting and to  
 26 understand how the interactions were related to the behavior of the QBO.

27 **3. Higher-order Wavelet Analysis**

### 1 3.1 Wavelet-based Autobicoherence

2 Higher-order spectral analysis provides the opportunity to quantify nonlinearities and allows  
 3 the detection of interacting oscillatory modes within a time series. More specifically, nonlinearities  
 4 are quantified using bicoherence, a tool for measuring quadratic nonlinearities, where quadratic  
 5 nonlinearities imply that for frequencies  $f_1$ ,  $f_2$ , and  $f_3$  and corresponding phases  $\phi_1$ ,  $\phi_2$ , and  $\phi_3$   
 6 the sum rules

$$7 \qquad f_1 + f_2 = f_3 \qquad (3)$$

8 and

$$9 \qquad \phi_1 + \phi_2 = \phi_3 \qquad (4)$$

10 are satisfied. Whereas Eq. (3) implies frequency coupling, Eq. (4) implies phase coupling. To see  
 11 from where Eqs. (3) and (4) originate, let

$$12 \qquad X(t) = \sin(2\pi f_1 t + \phi_1) + \sin(2\pi f_2 t + \phi_2) \qquad (5)$$

13 be the input into a system whose output is related to the input by

$$14 \qquad Y(t) = X(t) + \varepsilon X(t)^2 + w(t). \qquad (6)$$

15 The multiplicative factor  $\varepsilon$  is used to represent the contribution of the nonlinear component of the  
 16 signal and  $w(t)$  is Gaussian white noise. Note that if  $\varepsilon = 0$ , then the system is linear because the  
 17 output contains the same frequency components as the input. The substitution of Eq. (5) into Eq.  
 18 (6) results in

$$19 \qquad Y(t) = \sin(2\pi f_1 t + \phi_1) + \sin(2\pi f_2 t + \phi_2) + \frac{\varepsilon}{2} [1 - \cos(2(2\pi f_1 t + \phi_1)) \\
 20 \qquad - \cos(2(2\pi f_2 t + \phi_2)) + \cos(2\pi(f_2 - f_1)t + \phi_2 - \phi_1) \\
 21 \qquad - \cos(2\pi(f_1 + f_2)t + \phi_1 + \phi_2)] + w(t) \qquad (7)$$

22 and thus the output has sinusoids with additional frequency components  $2f_1$ ,  $2f_2$ ,  $f_2 - f_1$ , and  $f_2$   
 23  $+f_1$ , which arise from the second term in right-hand side of Eq. (6).

24 Unlike the power spectrum, which is the Fourier transform of the second-order moment of  
 25 a time series, the bispectrum is defined as the double Fourier transform of the third-order moment,  
 26 or, more generally, the third-order cumulant, i.e.,

1 
$$b_{xxx}(f_1, f_2) = \int_{-\infty}^{\infty} \int_{-\infty}^{\infty} C(t_1, t_2) e^{-i2\pi(f_1 t_1 + f_2 t_2)} dt_1 dt_2, \quad (8)$$

2 where  $C$  is the third-order cumulant, defined as

3 
$$C(t_1, t_2) = M_3(t_1, t_2) + M_1[M_2(t_1) + M_2(t_2) + M_2(t_1 - t_2)] + 2M_1^3 \quad (9)$$

4 and the  $t_i$  are lags. If  $X(t)$  is zero-mean, then in Eq. (9),  $M_1 = E[X(t)] = 0$  denotes the first-order  
 5 moment (mean),  $M_2 = E[X(t)X(t + t_1)]$  denotes the second-order moment (autocorrelation),  
 6 and  $M_3(t_1, t_2) = E[X(t)X(t + t_1)X(t + t_2)]$  denotes the third-order moment (Nidal and Malik,  
 7 2013). Also note that for a zero-mean process, the third-order cumulant reduces to the third-order  
 8 moment (Collis et al., 1998). A more useful quantity is the normalized version of the bispectrum,  
 9 the autobicoherence spectrum (Collis et al., 1998), which can be computed using the following:

10 
$$b^2(f_1, f_2) = \frac{|b_{xxx}(f_1, f_2)|^2}{E[|X_f(f_1)X_f(f_2)|^2]E[|X_f(f_1 + f_2)|^2]}, \quad (10)$$

11 where  $b^2(f_1, f_2)$  is bounded by 0 and 1 by the Schwarz inequality and  $X_f$  denotes the Fourier  
 12 transform of  $X$ .  $b^2(f_1, f_2)$  can be interpreted as the fraction of power at  $f_1 + f_2$  due to quadratic  
 13 phase coupling among  $f_1$ ,  $f_2$ , and  $f_1 + f_2$  such that the sum rule  $f_1 + f_2 = f_3$  is satisfied (Elgar  
 14 and Chandran, 1993). For a more in-depth discussion of higher-order spectral analysis the reader  
 15 is referred to Nikias and Raghuveer (1987).

16 Phase information and cycle geometry can be obtained from the biphas, which is given  
 17 by

18 
$$\psi = \tan^{-1} \left( \frac{\text{Im}(b_{xxx})}{\text{Re}(b_{xxx})} \right) = \phi_1 + \phi_2 - \phi_3. \quad (11)$$

19 It was noted by Maccarone (2013), however, that the biphas should be defined on the full  $2\pi$   
 20 interval and thus in this paper the four-quadrant inverse tangent is computed and not the inverse  
 21 tangent as shown above. By doing so, statistically significant autobicoherence detected together  
 22 with the biphas can be used to quantify cycle geometry. A biphas of  $0^\circ$  indicates positive  
 23 skewness and a biphas of  $180^\circ$  indicates negative skewness (Maccarone, 2013). An example of a  
 24 skewed oscillation time series with biphas close to  $0^\circ$  is shown in Fig. 2a. Mathematically, the  
 25 time series is written as

26 
$$X(t) = \sum_{j=1}^{40} \frac{1}{j} \cos[0.1jt + a(j - 1)], \quad (12)$$

1 where  $a = 0$  (Maccarone, 2013). The time series is skewed because the positive spikes are not  
 2 accompanied by negative spikes of equivalent magnitude and therefore the distribution of the time  
 3 series would be positively skewed, with the right tail being larger than the left tail.

4 For asymmetric waveforms, a biphasic of  $90^\circ$  indicates that the time series is linearly rising  
 5 but rapidly falling as shown in Fig. 3, whereas a biphasic of  $-90^\circ$  indicates that the time series rises  
 6 rapidly and falls linearly. A purely asymmetric time series will have a biphasic of  $90^\circ$  or  $-90^\circ$ , as  
 7 shown in Fig. 3, where the saw-toothed time series obtained by setting  $a = \pi/2$  in Eq. (12) rises  
 8 more slowly than it falls. In a physical setting, asymmetric cycle geometry implies that phase  
 9 transitions occur at different rates, as observed in the QBO time series.

10 According to Elsayed (2006), the wavelet-based autocorrelation is defined as

$$11 \quad b_{xxx}^w(s_1, s_2) = \frac{|B_{xxx}^w(s_1, s_2)|^2}{(\int_T |W_x(s_1, t)W_x(s_2, t)|^2 dt)(\int_T |W_x(s, t)|^2 dt)}, \quad (13)$$

12 where

$$13 \quad B_{xxx}^w(s_1, s_2) = \int_T W_x^*(s, t) W_x(s_1, t)W_x(s_2, t) dt, \quad (14)$$

$$14 \quad \frac{1}{s_1} + \frac{1}{s_2} = \frac{1}{s}, \quad (15)$$

15  
 16  $T$  is a time interval,  $W_x(s, t)$  is the wavelet transform of a time series  $X$  at scale  $s$  and time  $t$ , and  
 17  $W_x^*(s, t)$  denotes the complex conjugate of  $W_x(s, t)$ . The wavelet-based autocorrelation measures  
 18 the degree of quadratic phase coupling, where a peak at  $(s_1, s_2)$  indicates a statistical dependence  
 19 among the scale components  $s_1$ ,  $s_2$ , and  $s$ .

20 In practice, the autocorrelation is computed discretely so that Eq. (13) can be written as

$$21 \quad \overline{W}_b(s_1, s_2) = \frac{|B_{xxx}^w(s_1, s_2)|^2}{(\sum_{n=n_1}^{n_2} |W_n^X(s_1)W_n^X(s_2)|^2)(\sum_{n=n_1}^{n_2} |W_n^X(s)|^2)}, \quad (16)$$

22 where

$$23 \quad B_{xxx}^w(s_1, s_2) = \sum_{n=n_1}^{n_2} W_n^{*X}(s)W_n^X(s_1)W_n^X(s_2)$$



$$= \sum_{n=n_1}^{n_2} B_n^W(s_1, s_2), \quad (17)$$

$n_1 \geq 1$ , and  $n_2 \leq N$ . Note that if  $n_1 = 1$  and  $n_2 = N$ , then Eq. (16) represents the global autobicoherence spectrum.

The Monte Carlo approach to pointwise significance testing is adopted in this paper and is similar to that used in wavelet coherence (Grinsted et al., 2014). To estimate the significance of wavelet-based autobicoherence at each point  $(s_1, s_2)$ , Monte Carlo methods are used to (1) generate a large ensemble of red-noise processes with the same lengths and lag-1 autocorrelation coefficients as the input time series and (2) compute for each randomly generated red-noise process the autobicoherence spectrum. From the ensemble of autobicoherence spectra, the  $p = 100(1 - \alpha_p)$  percentile of the autobicoherence estimates is computed for every point  $(s_1, s_2)$ , where  $p$  corresponds to the critical level of the test and  $\alpha_p$  is the pointwise significance level of the test. Given the symmetry of the autobicoherence spectrum, the critical level of the test can be computed using only half of the autobicoherence estimates, reducing computational costs.

### 3.2 Multiple Testing

Let  $\alpha_p$  be the significance level of the pointwise significance test as described above and let  $K$  denote the number of autobicoherence estimates being tested, then there will be on average  $\alpha_p K$  false positive results. A similar problem occurs in traditional wavelet analysis (Maraun et al., 2007; Schulte et al., 2015; Schulte, 2016). In the case of simultaneously testing multiple hypotheses, the number of false positive results can be reduced by applying, for example, the Bonferroni correction (Lehmann, 1986). However, this simple correction often results in many true positives being rejected and is especially permissive in the case of autocorrelated data (Maraun et al., 2004). Other procedures also exist, including the Walker  $p$ -value adjustment procedure, which has more statistical power than the Bonferroni correction. An even more powerful method is the Benjamini and Hochberg (1995) procedure, which controls the false discovery rate (FDR), where the FDR is the expected proportion of the false rejections that are actually true. An advantage of this method, in addition to its statistical power, is that it takes into account the confidence with which local hypotheses are rejected and is robust even in the case of autocorrelated data (Wilks, 2002). Benjamini and Yekutieli (2001) developed a modified version of the Benjamini

1 and Hochberg (1995) procedure that works for any dependency structure among the local test  
 2 statistics and thus this procedure will be used in this paper to control the FDR.

3 The procedure can be described as follows: Suppose that  $K$  local hypotheses were tested.  
 4 Let  $p_{(i)}$  denote the smallest of the  $K$  local  $p$ -values, then, under the assumption that the  $K$  local  
 5 tests are independent, the FDR can be controlled at the  $q$ -level by rejecting those local tests for  
 6 which  $p_{(i)}$  is no greater than

$$\begin{aligned}
 7 \quad p_{FDR} &= \max_{j=1, \dots, k} [p_{(j)} : p_{(j)} \leq q(j/K)] \\
 8 \quad &= \max_{j=1, \dots, k} [p_{(j)} : p_{(j)} \leq \alpha_{global}(j/K)] \quad (18)
 \end{aligned}$$

9 so that the FDR level is equivalent to the global test level. For a local  $p$ -value to be deemed  
 10 significant using this procedure, it must be less than or equal to the largest  $p$ -value for which Eq.  
 11 (18) is satisfied. If no such local  $p$ -values exist, then none are deemed insignificant, and, therefore,  
 12 the global test hypothesis cannot be rejected. If the test statistics have an unknown dependency  
 13 structure,  $q$  can be replaced with  $q / \sum_{i=1}^K \frac{1}{i}$ , though this substitution makes the procedure less  
 14 powerful (Reiner et al., 2002). This modified method will be applied to autobicoherence spectra  
 15 at the 0.05 level throughout this paper.

### 16 **3.3 Wavelet-based Autobicoherence of an Idealized Time Series**

17 To demonstrate the features of a time series that can be extracted using higher-order  
 18 wavelet analysis, an idealized nonstationary time series will first be considered. Consider the  
 19 quadratically nonlinear time series

$$20 \quad X(t) = \cos(2\pi ft + \phi) + \gamma(t)\cos(4\pi ft + 2\phi) + w(t), \quad (19)$$

21 where  $f$  is frequency,  $w(t)$  is Gaussian white noise, and  $\gamma(t)$  is a time-dependent nonlinear  
 22 coefficient given by

$$23 \quad \gamma(t) = 0.001t. \quad (20)$$

24 Note that Eqs. (3) and (4) are satisfied because  $f_1 + f_2 = 2f_1 = 2f_2$  and similarly for  $\phi$ . The  
 25 sinusoid with frequency  $2f_1$  is said to be the harmonic of the primary frequency component with  
 26 frequency  $f_2$ , where the amplitude of the harmonic depends on  $\gamma(t)$ , the strength of the quadratic

1 nonlinearity.  $X(t)$  and the corresponding wavelet power spectrum for the case when  $f_1 = 0.03$  is  
2 shown in Fig. 4. The signal-to-noise ratio of the Gaussian white noise was set to 1 decibels. The  
3 primary frequency component results in a large region of 5% pointwise significance at  $\lambda = 30$ ,  
4 whereas its harmonic only results in a few small significance regions located from  $t = 700$  to  $t =$   
5 1000. It also noted that the appearance of the significance power at  $\lambda = 15$  from  $t = 700$  to  $t =$   
6 1000 is accompanied by large positive spikes in the time series that result in the time series  
7 favoring positive values. Prior to the emergence of the significant power at  $\lambda = 15$ , the time series  
8 varied smoothly in the sense that negative phases were accompanied by positive phases of similar  
9 amplitude.

10 To determine if the oscillations are quadratically interacting, the autobicoherence of  $X(t)$   
11 was computed (Fig. 5). The significant peak centered at (30, 30) indicates that an oscillation with  
12 period 30 is phase-coupled to an oscillation with  $\lambda = 15$ . The result implies that the variability at  
13  $\lambda = 15$  is partially related to the statistical dependence between the two modes. The fraction of  
14 variability is determined by the autobicoherence value corresponding to the significant peak. In  
15 the present case,  $\overline{W}_b(s_1, s_2) = 0.5$  so about half of the variability at  $\lambda = 15$  is due to the nonlinear  
16 interaction. Note that no other peaks were found to be significant.

### 17 **3.4 Wavelet-based Autobicoherence of Geophysical Time Series**

18 Shown in Fig. 6 is the wavelet-based autobicoherence spectrum for the QBO time series.  
19 A large region of significance was identified, which contained the local maximum at (28, 28)  
20 months. The peak represents the phase coupling of the primary frequency component with its  
21 harmonic with a period of 14 months. The power at  $\lambda = 14$  months therefore is partially related to  
22 the statistical dependence between its primary frequency component and its harmonic. The  
23 significance and magnitude of the autobicoherence in the QBO spectrum is consistent with how  
24 the QBO does not vary smoothly, shifting to the easterly phase more quickly than to the westerly  
25 phase and with the westerly phase tending to be stronger than the easterly phase. The asymmetry  
26 in both phase transition and magnitude are suggestive of nonlinearities.

### 27 **3.5 Local Wavelet Autobicoherence**

28 It may also be desirable to see how autobicoherence along slices of the full autobicoherence  
29 spectrum changes with time. To compute local autobicoherence, apply a smoothing operator  $S(W)$

1 =  $S_{scale} \left( S_{time} (W_n^X(s)) \right)$  (Grinsted et al., 2004) to each term in Eq. (13) instead of summing in  
 2 time, i.e.,

$$3 \quad b_n^w(s_1, s_2) = \frac{|S(s_1^{-1} B_n^w(s_1, s_2))|^2}{S(s_1^{-1} |W_n^X(s_1) W_n^X(s_2)|^2) \cdot S(s^{-1} |W_n^X(s)|^2)}. \quad (20)$$

4 The smoothing operator for the Morlet wavelet is given by

$$5 \quad S_{time}(W)|_s = \left( W_n^X(s) * c_1 \frac{-t^2}{2s^2} \right) |_s \quad (21)$$

6 and

$$7 \quad S_{scale}(W)|_n = (W_n^X(s) * c_2 \Pi(.6s))|_n, \quad (22)$$

8 where  $c_1$  and  $c_2$  are normalization constants determined numerically and  $\Pi$  is the rectangular  
 9 function.

10 It is important to mention that the numerator of Eq. (20) contains a term with wavelet  
 11 coefficients at two different scales so that the choice of smoothing is not as straightforward as for  
 12 wavelet coherence. Smoothing autobicoherence estimates with respect to  $s_{min} = \min(s_1, s_2)$  was  
 13 found to result in larger autobicoherence estimates, whereas smoothing the autobicoherence with  
 14 respect to  $s_{max} = \max(s_1, s_2)$  resulted in smaller autobicoherence estimates. Given that the  
 15 autobicoherence estimates are influenced by the choice of smoothing, it is inevitable that the  
 16 significance of the autobicoherence estimates is also impacted. In particular, smoothing the  
 17 autobicoherence spectrum with respect to  $s_{max}$  allowed extrema to be smoothed out, eliminating  
 18 spuriously large autobicoherence. For this reason, all local autobicoherence spectra in this paper  
 19 will be computed by smoothing with respect to  $s_{max}$ .

20 The advantage of using Eq. (20) is that transient quadratic nonlinearities can now be  
 21 detected and the need for choosing an integration time interval has been eliminated. If  $s_1 = s_2$ , then  
 22  $(t, s_1, s_1) = (t, s_2, s_2) = (t, s)$  and thus, in the case of this diagonal slice, the local wavelet-based  
 23 bicoherence spectrum is a two-dimensional representation of the degree of local quadratic  
 24 nonlinearity. The vertical axis corresponds to the primary frequency and the horizontal axis  
 25 corresponds to time. As a concrete example, a peak at (64, 64) would indicate that at time index  $t =$

1 50 the oscillation with a fundamental period  $\lambda = 1.03s \approx 64$  is locally coupled to an oscillation  
2 with period  $\lambda \approx 32$ .

3 One can also compute a local biphas from the smoothed bispectrum by taking the four  
4 quadrant inverse tangent of the smoothed imaginary part divided by the smoothed real part. The  
5 local biphas, for example, was computed for the skewed time series shown in Fig. 2a. As  
6 expected, the biphas fluctuates regularly around  $0^\circ$  and the mean is  $2^\circ$ . The local biphas for the  
7 saw-toothed time series is shown in Fig. 3b. The biphas fluctuates about  $90^\circ$  and the mean biphas  
8 is  $90^\circ$  as expected.

9 The procedure for the estimation of the statistical significance of local autobicoherence is  
10 the following: generate red-noise time series with the same lag-1 autocorrelation coefficients as  
11 the input time series and use the local autobicoherence estimates outside the COI to generate a null  
12 distribution of  $b_n^w(s_1, s_2)$ . Note that the calculation only needs to be performed at a fixed time  
13 outside of the COI because red-noise is a stationary process, which produces a stationary  
14 background spectrum.

### 15 **3.6 Local Wavelet-based Autobicoherence of an Idealized Time Series**

16 The local autobicoherence spectrum of  $X(t)$  for (30, 30) is shown in Fig. 6b. Initially, there  
17 is no local autobicoherence that exceeds the 5% significance level. At  $t = 250$  and  $t = 500$ , on the  
18 other hand, small regions of 5% significant autobicoherence emerge, indicating a transient  
19 nonlinear interaction. At  $t = 500$  the nonlinearity is strong and results in a large region of significant  
20 local autobicoherence extending from  $t = 500$  to the edge of the wavelet domain

21 In order to determine if the peaks in autobicoherence are associated with a quadratic  
22 nonlinearity, it is important to compute the biphas, which is shown in Fig. 7b. From  $t = 0$  to  $t =$   
23 400 there is an unstable phase relationships between the phase of the primary frequency component  
24 and its harmonic. Such a lack of phase coherence indicates a weak nonlinear interaction, which is  
25 consistent with how the autobicoherence is lower before  $t = 400$ . In contrast, after  $t = 400$ , the  
26 biphas becomes stable, changing little with time, indicating a consistent phase relationship  
27 between the primary frequency mode and its harmonic. It also noted that the biphas during this  
28 time fluctuates near  $0^\circ$ , which implies that the phase relationships arise from a quadratic  
29 nonlinearity. The near zero biphas is consistent with how  $X(t)$  was constructed from the sum of

1 two cosines with zero phase and also suggests that the interaction results in skewed cycle geometry,  
2 where positive values of the time series are preferred. Indeed, by inspection of Fig. 4a the  
3 oscillations initially appear to be sinusoidal, varying smoothly, whereas after  $t = 400$  spikes begin  
4 to appear and  $X(t)$  favors positive values.

### 5 **3.7 Local Wavelet-based Autobi-coherence of the QBO Time Series**

6 The local autobi-coherence spectrum of the QBO index at the point (28, 28) in the full  
7 autobi-coherence spectrum is shown in Fig. 8. From 1950 to 1970 the magnitude of the  
8 autobi-coherence fluctuated and consisted of one local significant peak at 1965. Significant  
9 autobi-coherence was also found from 1975 to 1998, contrasting with the autobi-coherence after  
10 1998, which was not found to be significant until 2010.

11 To determine if the peaks indicated in the autobi-coherence are associated with a quadratic  
12 nonlinearity, the local biphas was computed. Fig. 8a shows the local biphas for the  
13 autobi-coherence peak at (28, 28). For most of the study period, the biphas was found to vary  
14 considerably, particularly during the 1950-1970 and 1995-2013 periods. On the other hand, the  
15 biphas varied smoothly from 1970 to 1995, consistent with how the autobi-coherence during that  
16 period was large and stable (Fig. 8a). Also, during that period the biphas was nonzero; in fact, the  
17 mean biphas during the period was  $-100^\circ$ , suggesting that the phase coupling is not the result of  
18 a quadratic interaction. A biphas of  $-100^\circ$  indicated asymmetric geometry, which physically  
19 represents how phase transitions of the QBO occurred at different rates. Recall that it has already  
20 been discussed in the introduction that the QBO transitions from easterly phases to westerly phases  
21 more rapidly than from westerly to easterly phases (Lu et al., 2009). Another interesting feature is  
22 the general increase in the biphas from 1970 to 1995. In the beginning of the time period, the  
23 biphas was  $-180^\circ$  and after 1980 the biphas switched to  $-90^\circ$ .

24 The local autobi-coherence and biphas corresponding to the peak (16, 26) was also  
25 computed (Fig. 9). The mean of the absolute value of the biphas for the period 1950-2013 was  
26  $130^\circ$ , indicating a statistical dependency among the modes with periods of 10, 16, 26 months  
27 resulted in skewed waveforms. In fact, because the biphases were close to  $180^\circ$  the waveforms  
28 should have been skewed to negative values (Maccarone, 2013) and such skewness is evident by  
29 inspecting Fig. 1. Also note that some of the largest negative phases of the QBO occurred from

1 1995 to 2010, which coincided with the period of most significant autobicoherence as shown in  
2 Fig. 9a.

### 3 **4. Block Bootstrapping Methods**

#### 4 **4.1 Block Bootstrapping Autobicoherence**

5         Bootstrapping is a widely used technique to estimate the variance or uncertainty of a  
6 sample estimate. For independent data one samples with replacement individual data points (Efron,  
7 1979); for dependent data one must sample with replacement blocks of data to preserve the  
8 autocorrelation structure of the data (Kunsch, 1989). The latter technique is called block  
9 bootstrapping and should be used for variance estimation of global wavelet quantities, as wavelet  
10 coefficients are known to be autocorrelated in both time and scale. The use of traditional  
11 bootstrapping techniques would result in confidence intervals that are too narrow. It is expected,  
12 however, that the choice of the bootstrapping technique is more critical at larger scales, as the  
13 decorrelation length of the mother wavelet increases with scale.

14         A brief overview of the procedure is provided below but a more detailed discussion can be  
15 found in Schulte et al. (2015). To find the approximate  $100(1 - \beta)\%$  confidence interval of an  
16 autobicoherence estimate, divide the set of wavelet coefficients at each scale into overlapping  
17 blocks. The lengths of the blocks at each scale should be the same and the randomly resampled  
18 blocks chosen should be the same at each scale to avoid randomizing the data. The concatenation  
19 of the blocks then results in a synthetic set of wavelet coefficients at each scale. The synthetic set  
20 of wavelet coefficients can then be used to calculate a bootstrap replicate of the autobicoherence.  
21 The iteration of the procedure 1000 times results in a distribution of bootstrap replicates from  
22 which a 95% confidence interval can be obtained.

23         As noted by Schulte et al. (2015), the appropriate block length to use can be determined by  
24 Monte Carlo methods. In that study, it was determined from a Monte Carlo experiment that a block  
25 length of  $N^{0.6}$  produced accurate confidence bounds for wavelet coherence while also producing  
26 the widest confidence intervals at all scales. The Monte Carlo experiment was repeated for 95%  
27 confidence in this study because bicoherence estimation requires the use of wavelet coefficients at  
28 three wavelet scales, with the wavelet coefficients at each scale having a different correlation  
29 structure. For wavelet coherence, the block length selection procedure is simpler because a single

1 wavelet scale is used so that correlation structure of wavelet coefficients is similar. The Monte Carlo  
2 experiment was performed by generating red-noise processes of length 1000 with different lag-1  
3 autocorrelation coefficients and computing 95% confidence intervals around the estimated  
4 autobicoherence. Remarkably, the Monte Carlo experiment found that a block length of  $N^{0.6}$  is  
5 also optimal for bicoherence confidence interval estimation. For block lengths exceeding  $N^{0.6}$ ,  
6 confidence intervals were found to be too narrow, with in some instances the estimated  
7 bicoherence falling outside the 95% confidence interval. It is also noted that the results were  
8 insensitive to the chosen lag-1 autocorrelation coefficient.

#### 9 **4.4.2 Application to Ideal and Climatic Time Series**

10 Figure 5b shows the application of the block bootstrap procedure to the diagonal slice  $s_1 =$   
11  $s_2 = s$  of the autobicoherence for the ideal case. The 95% confidence intervals were also obtained  
12 using the ordinary bootstrap method. A pronounced peak at  $s = 30$  was identified and represents  
13 the interaction between the primary frequency and its harmonic. By inspection of Fig. 5b, there is  
14 a clear difference between the widths of the confidence intervals obtained from the two  
15 bootstrapping procedures. For the ordinary bootstrap, the confidence intervals are narrow and the  
16 widths of the confidence intervals appear to be only weakly dependent on scale. On the other hand,  
17 the confidence intervals obtained using the block bootstrap procedure are wide, especially at large  
18 scales, and the width of the confidence intervals depends strongly on scale, increasing from small  
19 scales to large scales. It is also noted that, whereas the block bootstrap procedure has deemed no  
20 spurious peaks as significant, the ordinary bootstrap procedure deemed two the spurious peaks at  
21  $s = 14$  and  $s = 100$  as significant. The implementation of the block bootstrap procedure can  
22 therefore enhance confidence in results, facilitating the investigation of a deeper physical  
23 understanding.

24 The application of the block bootstrap procedure to the diagonal slice  $s_1 = s_2 = s$  of the  
25 full autobicoherence spectrum of the QBO index is shown in Fig 10. The 95% confidence intervals  
26 corresponding to the peaks (14, 14) and (28, 28) do not cross the 5% significance bound and thus  
27 one has more confidence that those peaks are significant. All other peaks have been deemed  
28 insignificant.

## 29 **5. Summary**



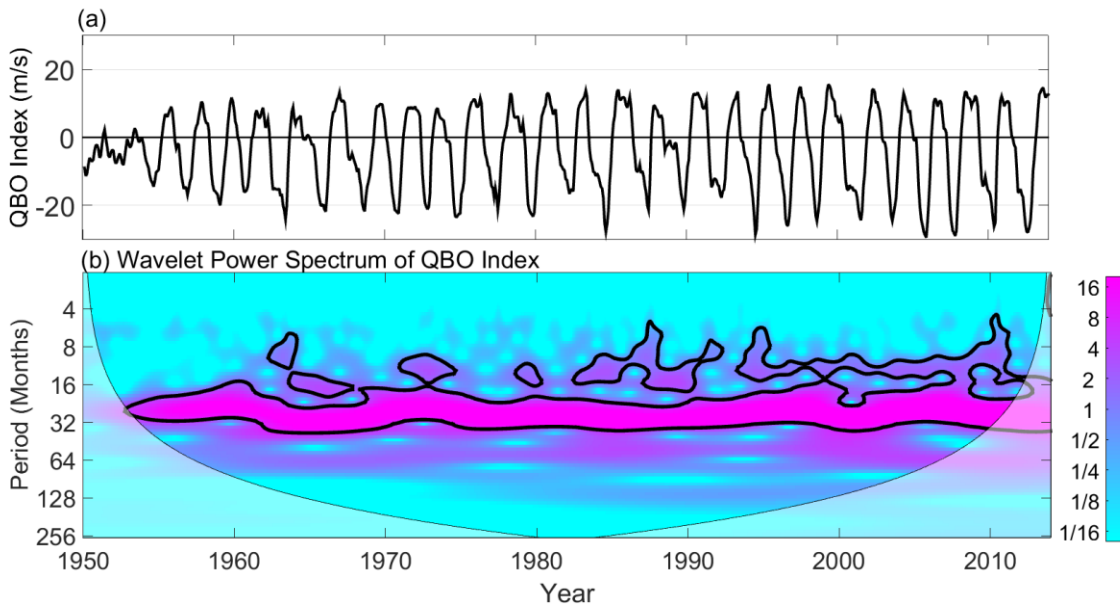
1 Higher-order wavelet analysis together with significance testing procedures were used to  
2 detect nonlinearities embedded in an ideal time series and the QBO time series. The  
3 autobicoherence spectrum of the QBO index revealed phase coupling of the 28 month mode with  
4 a higher frequency mode with period 14 months. A local autobicoherence spectrum of the QBO  
5 index showed that the strength of the nonlinearities varied temporally. Furthermore, the local  
6 biphasic spectrum indicated that a statistical dependence among frequency components resulted in  
7 waveforms that were both skewed and asymmetric, indicating that the strength of negative QBO  
8 events were stronger than positive events, and that transitions between events occurred at different  
9 rates.

10

1 **Acknowledgements:** Support for this research was provided by the National Science Foundation  
2 Physical Oceanography Program (award number 0961423) and the Hudson River Foundation  
3 (award number GF/02/14).

4

1



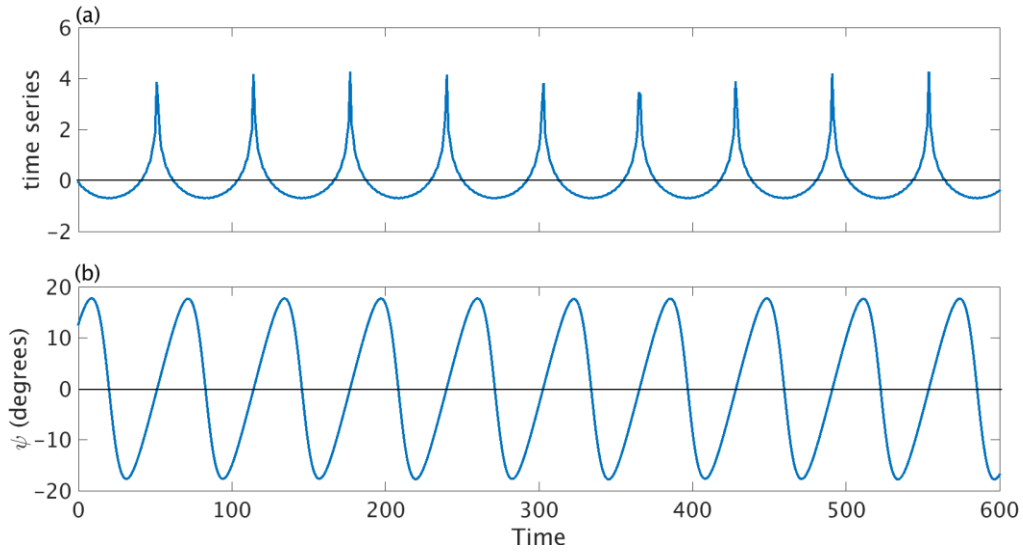
2

3 Figure 1. (a) The QBO index and (b) the corresponding wavelet power spectrum. Contours enclose  
4 regions of 5% statistical pointwise significance (Torrence and Compo, 1998). Light shading  
5 represents the cone of influence, the region in which edge effects cannot be ignored.

6

7

8

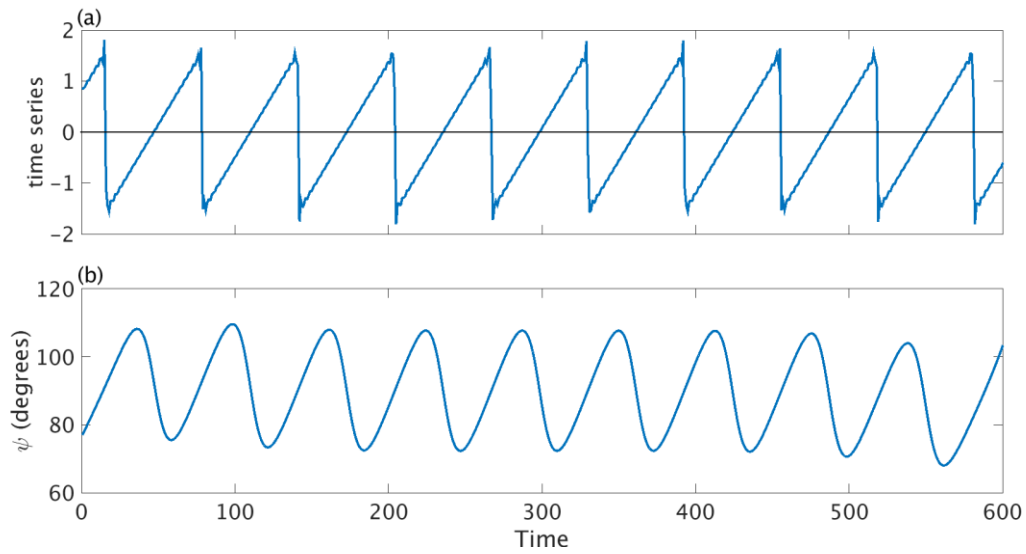


1

2 Figure 2. (a) a skewed time series and (b) its corresponding local biphaseness. The biphaseness close to  
 3 zero indicates a nonlinear interaction resulting in a skewed oscillation. The biphaseness was calculated  
 4 from the first three cosines in the summation described in the text. The large deviations from zero  
 5 at the edges are the result of edge effects.

6

1

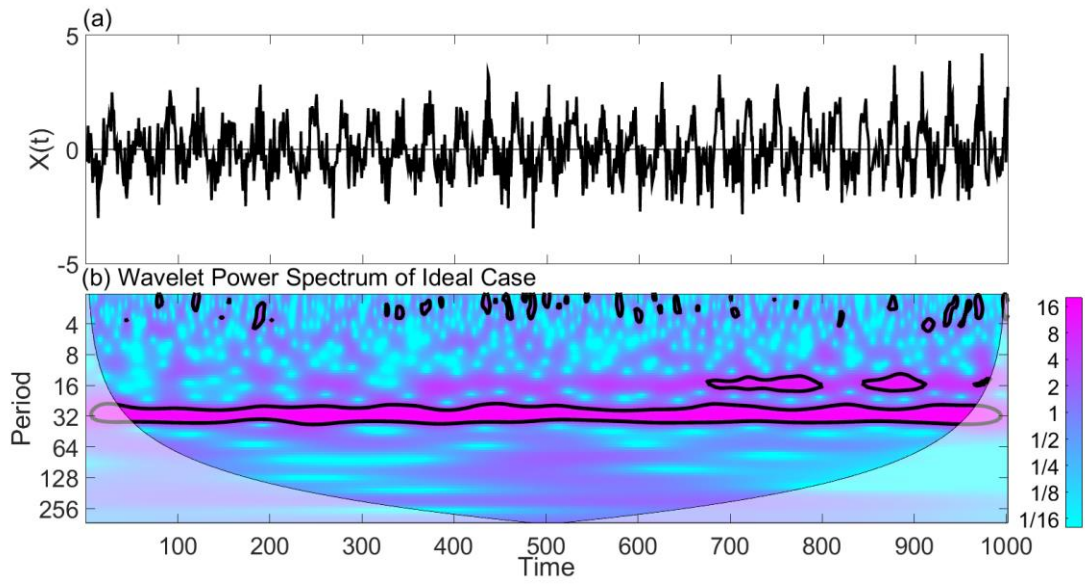


2

3 Figure 3. (a) A saw-toothed time series and (b) its corresponding local biphasic phase. The biphasic phase close  
4 to  $90^\circ$  indicates a nonlinear interaction resulting in an asymmetric waveform. The biphasic phase was  
5 calculated from the first three cosines in the summation.

6

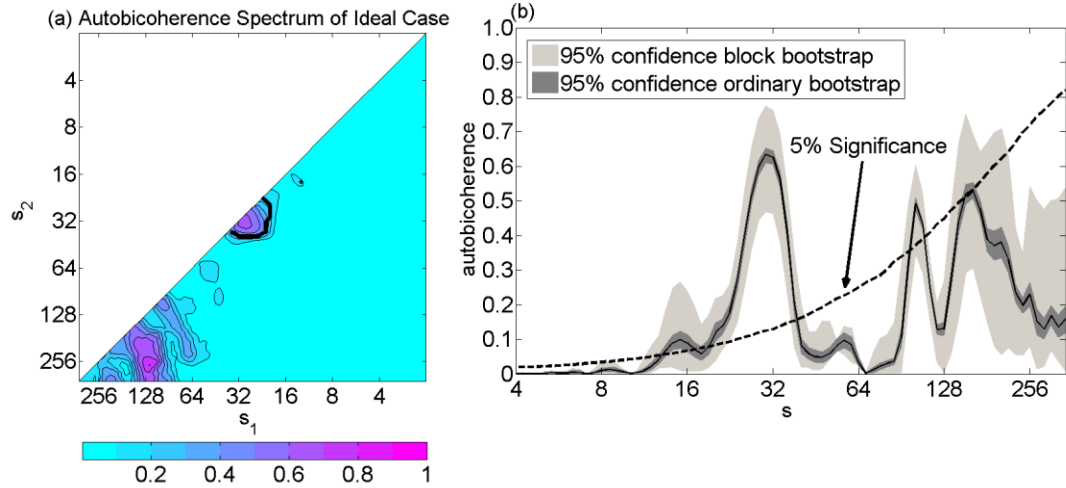
7



1

2 Figure 4. (a) Time series corresponding to Eq. (19). (b) Corresponding wavelet power spectrum.

3



1

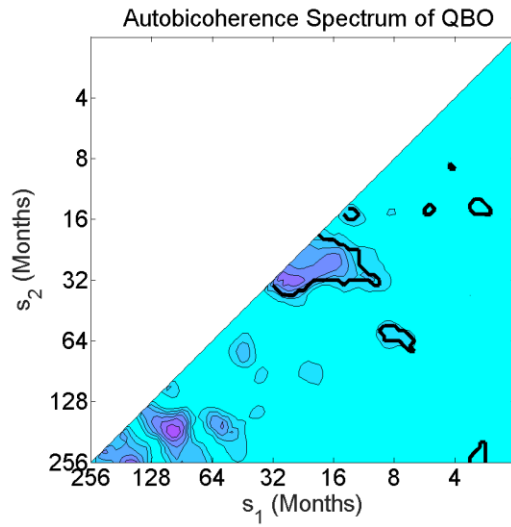
2 Figure 5. (a) Wavelet-based autobicoherence spectrum of the ideal time series. Thick contours  
 3 enclose regions of 5% pointwise significance after controlling the FDR. The diagonal line separates  
 4 the spectrum into two symmetric regions. (b) The diagonal slice of the autobicoherence spectrum  
 5 at  $s_1 = s_2 = s$ . The critical level for the test represented by the dotted line was calculated using  
 6 Monte Carlo methods.

7

1

2

3



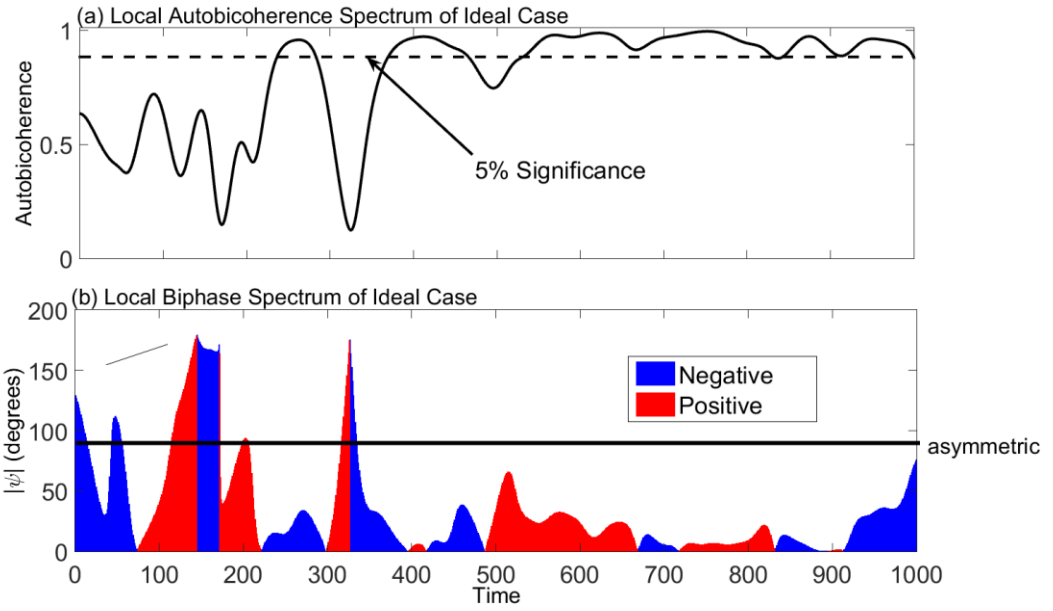
4

5 Figure 6. The wavelet-based autobicoherence spectrum of the QBO index for the period 1950-  
6 2013. Thick contours enclose regions of 5% pointwise significance.

7

8



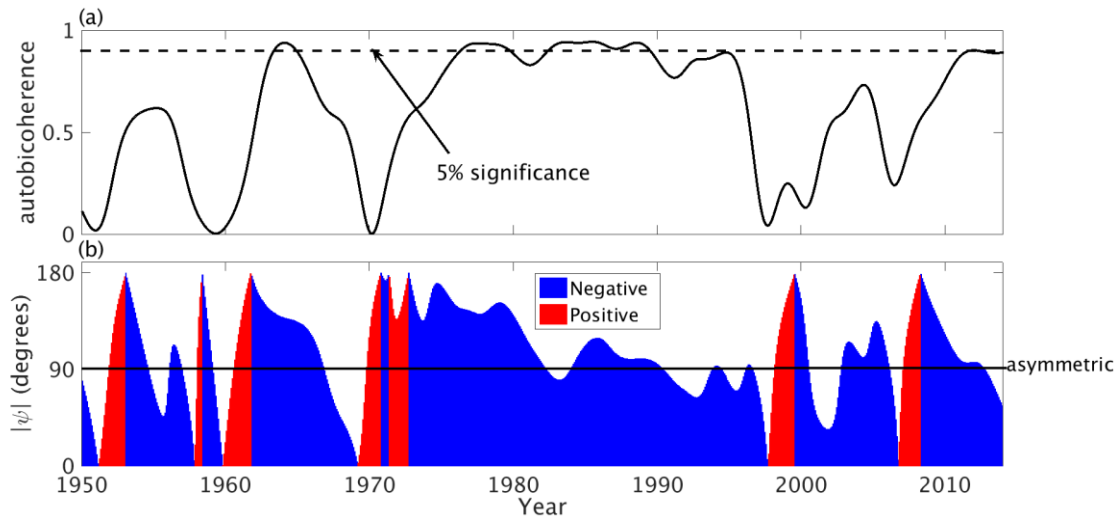


1

2 Figure 7. (a) The local autobi-coherence and (b) local biphas corresponding to (30, 30) in the full  
 3 autobi-coherence spectrum shown in Figure 5a. Biphases differing from  $90^\circ$  indicate that the  
 4 nonlinear interaction resulted in a waveform with skewness.

5

6

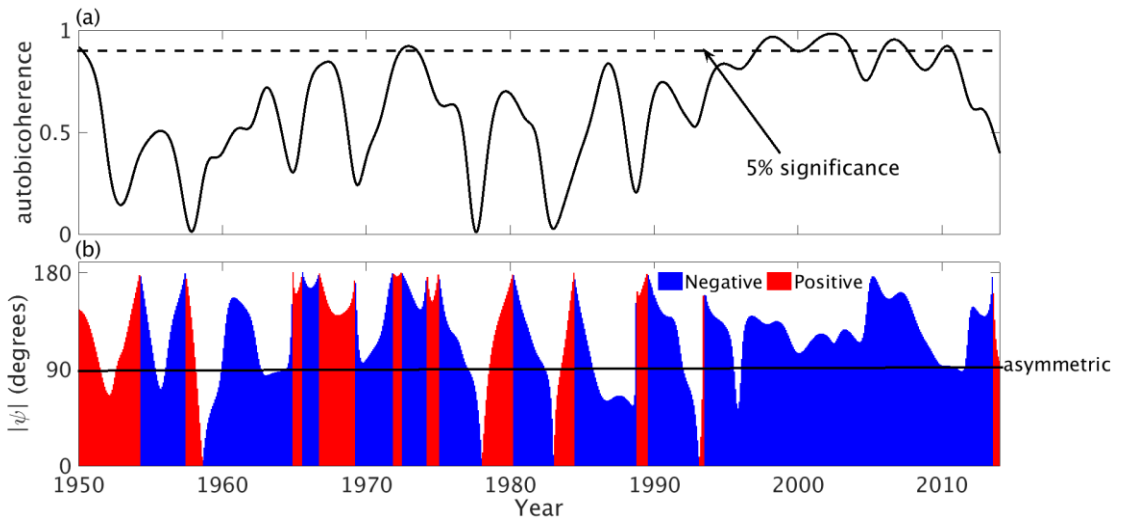


1

2 Figure 8. Same as Fig. 7 except at (28, 28) in the autocohereance spectrum of the QBO index  
 3 Biphases differing from  $90^\circ$  indicate that the nonlinear interaction resulted in a waveform with  
 4 skewness.

5

1

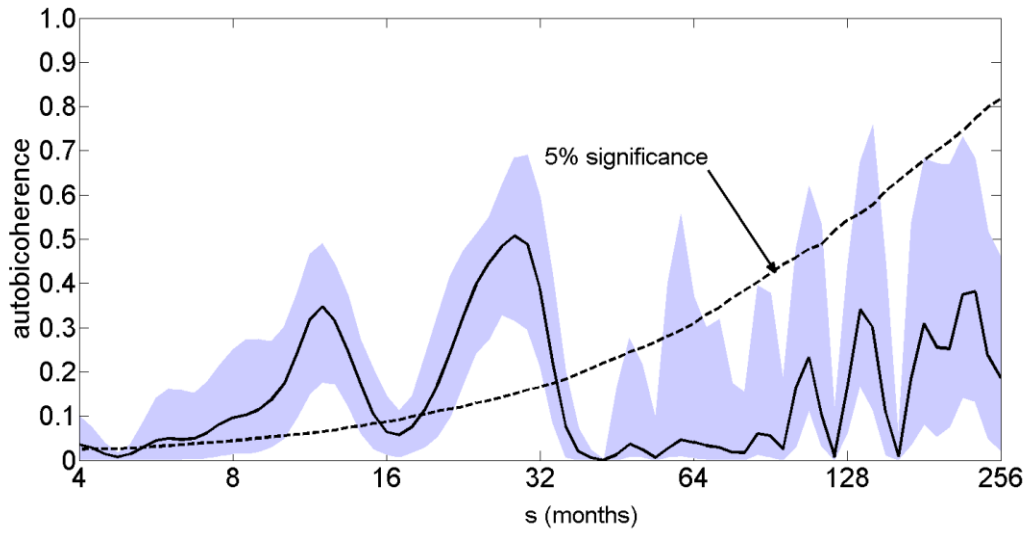


2

3 Figure 9. Same as Fig. 8 except at the point (16, 26).

4

5



1

2 Figure 10. Same as Fig. 5b except for the QBO index for the period 1950-2013.

3

4

1 **References**

- 2 Alley, R. B., Marotzke, J., Nordhaus, W. D, Overpeck, J. T., Peteet, D. M., Pielke Jr., R. A.,  
3 Pierrehumbert, R. T., Rhines, P. B., Stocker, T. F., Talley, L. D., Wallace, J. M.: Abrupt Climate  
4 Change. *Science*, 299, 2005-2010, 2003.
- 5 Benjamini, Y., Hochberg, Y.: Controlling the False Discovery Rate: A Practical and Powerful  
6 Approach to Multiple Testing. *J. Royal Statistical Society*, 57, 289-300, 1995.
- 7 Benjamini, Y., Yekutieli, D.: The Control of the False Discovery Rate in Multiple Testing under  
8 Dependency. *Ann. Statist.*, 29, 1165-1188, 2001.
- 9 Collis, W. B., White, P. R. and Hammond, J. K.: Higher-order Spectra: The Bispectrum and  
10 Trispectrum. *Mech. Syst. Signal Process.* 12, 375–394, 1998.
- 11 Efron, B.: Bootstrap Methods: Another Look at the Jackknife. *Ann. Statist.*, 7, 1–26, 1979.
- 12 Elgar, S. and Chandran, V.: Higher-order Spectral Analysis to Detect Nonlinear Interactions in  
13 Measured Time Series and an Application to Chua’s Circuit. *Internat. J. Bifurcat. Chaos*, 3, 19–  
14 34, 1993.
- 15 Elgar, S. and Sebert, G.: Statistics of Bicoherence and Biphas. *J. Geophysical Research*, 94,  
16 10993-10998, 1989.
- 17 Elsayed, M. A. K.: Wavelet Bicoherence Analysis of Wind–wave Interaction. *Ocean Eng.*, 33,  
18 458–470, 2006.
- 19 Gan, T. Y., Gobena, A. K., and Wang, Q.: Precipitation of Southwestern Canada: Wavelet,  
20 Scaling, Multifractal Analysis, and Teleconnection to Climate Anomalies, *J. Geophys. Res.*, 112,  
21 D10110,
- 22 Grinsted, A., Moore, J. C. and Jevrejeva, S.: Application of the Cross Wavelet Transform and  
23 Wavelet Coherence to Geophysical Time Series. *Nonlinear Process. Geophys.*, 11 , 561–566,  
24 2004.
- 25 Hagelberg, T., Piasias, N., Elgar, S.: Linear and Nonlinear Couplings between Orbital Forcing and  
26 the Marine  $\delta^{18}\text{O}$  Record during the Late Neocene. *Paleoceanography*, 6, 729-746, 1991.  
27
- 28 Hamilton, K. and Hsieh, W. W.: Representation of the Quasi-biennial Oscillation in the Tropical  
29 Stratospheric Wind by Nonlinear Principal Component Analysis. *J. Geophys. Res.*, 107, 4232,  
30 doi:10.1029/2001JD001250, 2002.
- 31 Higuchi, K., Huang, J., Shabbar, A.: A Wavelet Characterization of the North Atlantic Oscillation  
32 Variation and its Relationship to the North Atlantic Sea Surface Temperature. *Int. J. Climatol.*, 19,  
33 1119-1129, 1999.

1  
2 Jevrejeva, S., Moore, J. C., Grinsted, A.: Influence of the Arctic Oscillation and El Nino-Southern  
3 Oscillation (ENSO) on Ice Conditions in the Baltic Sea: The wavelet Approach. *J. Geophys. Res.*,  
4 108, 4677, doi:10.1029/2003JD003417, D21, 2003.  
5  
6 King, T.: Quantifying Nonlinearity and Geometry in Time Series of Climate. *Quat. Sci. Rev.*, 15,  
7 247–266, 1996.  
8  
9 Kunsch, H. R.: The Jackknife and the Bootstrap for General Stationary Observations. *Ann. Statist.*,  
10 17, 1217–1241, 1989.  
11  
12 Labat, D.: Cross Wavelet Analyses of Annual Continental Freshwater Discharge and Selected  
13 Climate Indices. *J. Hydrol.*, 385, 269-278, 2010.  
14  
15 Lee, Y. J., Lwiza, K. M.: Factors Driving Bottom Salinity Variability in the Chesapeake Bay. *Cont.*  
16 *Shelf Res.*, 28, 1352-1362, 2008.  
17  
18 Lu, B.W., Pandolfo, L., and Hamilton, K.: Nonlinear Representation of the Quasi-Biennial  
19 Oscillation. *J. Atmos. Sci.*, 66, 1886–1904, 2009.  
20  
21 Maccarone, T. J.: The Biphase Explained: Understanding the Asymmetries in Coupled Fourier  
22 Components of Astronomical Timeseries, *Mon. Not. R. Astron. Soc.*, 435, 3547, doi:  
23 10.1093/mnras/stu1824, 2013.  
24  
25 MacDonald, G. M., Case, R. A.: Variations in the Pacific Decadal Oscillation over the Past  
26 Millennium, *Geophys. Res. Lett.*, 32, L08703, doi:10.1029/2005GL022478, 2005.  
27  
28 Maraun, D., Kurths, J., and Holschneider, M.: Nonstationary Gaussian Processes in the Wavelet  
29 Domain: Synthesis, Estimation, and Significance Testing, *Phys. Rev. E*, 75, doi: 2  
30 10.1103/PhysRevE.75.016707, 2007.  
31  
32 Moussas, X., Polygiannakis, J. M., Preka-Papadema, P., Exarhos, G., Solar cycles: A tutorial. *Adv.*  
33 *Sp. Res.*, 35, 725-738, 2005.  
34  
35 Newman, M., Compo, G. P., Alexander, M. A.: ENSO-forced variability of the Pacific decadal  
36 oscillation. *J. Climate*, 16, 3853-3857, 2003.  
37  
38 Nidal, K. and Malik, A. S.: EEG/ERP Analysis: Methods and Applications, CRC Press, 334 pp.,  
39 2013.  
40  
41 Nikias, C. L., Raghuvver, M. R.: Bispectrum Estimation: A Digital Signal Processing Framework,  
42 *IEEE*, 75, 869-891, 1987.  
43  
44 Olsen, J., Anderson, J. N., Knudsen, M. F.: Variability of the North Atlantic Oscillation over the  
45 past 5,200 years, *Nature Geosci.*, 5, 808-812, 2012.

- 1 Polygiannakis, J. M., Moussas, X., Sonett, C. P. A Nonlinear RLC Solar Cycle Model. *Sol. Phys.*  
2 163, 193–203, 1996.
- 3 Polygiannakis, J., Preka-Papadema, P., Moussas, X.: On Signal–noise Decomposition of Time-  
4 series using the Continuous Wavelet Transform: Application to Sunspot Index. *MNRAS*, 343, 725-  
5 734, 2003.
- 6
- 7 Rial, J. A., Anaclerio, C. A.: Understanding Nonlinear Responses of the Climate System  
8 to Orbital Forcing. *Quat. Sci. Rev.*, 19, 1709-1722, 2000.
- 9
- 10 Rusu, M. V.: The Asymmetry of the Solar Cycle: A result of Non-linearity, *Adv. Sp. Res.*, 40,  
11 1904-1911, 2007.
- 12 Rutherford, S., D'Hondt, S.: Early Onset and Tropical Forcing of 100,000-year Pleistocene Glacial  
13 Cycles. *Nature*, 408, 72-75, 2000.
- 14
- 15 Schulte, J. A., Duffy, C., and Najjar, R. G.: Geometric and Topological Approaches to Significance  
16 Testing in Wavelet Analysis. *Nonlin. Processes Geophys.*, 22, 139-156, 2015.
- 17 Schulte, J. A., Najjar, R. G., Lee, S.: Salinity and Streamflow Variability in the Mid-Atlantic  
18 Region of the United States and its Relationship with Large-scale Atmospheric Circulation  
19 Patterns, *J. Hydrology*, submitted.
- 20
- 21 Schulte, J. A.: Cumulative areawise testing in wavelet analysis and its application to geophysical  
22 time series, *Nonlin. Processes Geophys.*, 23, 45-57, doi:10.5194/npg-23-45-2016, 2016.
- 23
- 24 Timmermann A.: Decadal ENSO Amplitude Modulations: a Nonlinear Paradigm. *Global Planet*  
25 *Change*, 37, 135-156, 2003.
- 26 Torrence, C. and Compo, G. P.: A Practical Guide to Wavelet Analysis, *Bull. Am. Meteorol. Soc.*,  
27 79, 61–78, 1998.
- 28 Torrence, C., Webster, P. J.: Interdecadal Changes in the ENSO–Monsoon System. *J. Climate*, 12,  
29 2679–2690, 1999.
- 30 Van Milligen, B. P., Sánchez, E., Estrada, T., Hidalgo, C., Brañas, B., Carreras, B., García, L.:  
31 Wavelet Bicoherence: A New Turbulence Analysis Tool. *Phys. Plasmas*, 2, 3017-3032, 1995.
- 32 Velasco, V. M. and Mendoza, B.: Assessing the Relationship between Solar Activity and Some  
33 Large Scale Climatic Phenomena, *Adv. Sp. Res.*, 42, 866–878, 2008.
- 34 Watson, P. A. G. and Gray, L. J.: How Does the Quasi-Biennial Oscillation Affect the  
35 Stratospheric Polar Vortex?. *J. Atmos. Sci.*, 71, 391–409, 2014.
- 36 Wilks, D. S.: Resampling Hypothesis Tests for Autocorrelated Fields. *J. Clim.*, 10, 65–82, 1997.

1

2

3

4